Journal of Magnetism and Magnetic Materials 505 (2020) 166734

Contents lists available at ScienceDirect

Journal of Magnetism and Magnetic Materials

journal homepage: www.elsevier.com/locate/jmmm

Research articles

A high performance magnetic fluid based on carbon modified magnetite (Fe_3O_4) nanospheres

Linfeng Bai[a,1], Lei Pei[b,1], Saisai Cao[b], Xiaokang He[b], Min Sang[a], Wanquan Jiang[a,*], Shouhu Xuan[b], Xinglong Gong[b,*]

[a] Department of Chemistry, University of Science and Technology of China, Hefei, Anhui 230026, PR China
[b] CAS Key Laboratory of Mechanical Behavior and Design of Materials, Department of Modern Mechanics, CAS Center for Excellence in Complex System Mechanics, University of Science and Technology of China, Hefei, Anhui 230027, China

ARTICLE INFO

Keywords:
Magnetic fluid
Fe_3O_4@C nanospheres
Crystallinity
Particle level dynamic simulation

ABSTRACT

This work reported a carbon layer modified magnetite (Fe_3O_4) nanospheres (Fe_3O_4@C) which could be applied in preparing high performance magnetic fluid. The porous Fe_3O_4@C nanospheres were prepared by calcinating the Fe_3O_4@Polydopamine (Fe_3O_4@PDA) precursor in N_2 atmosphere. The shear stress of Fe_3O_4@C-based magnetic fluid was as high as 24.9 Pa at saturated magnetic field, which was about 3.8 times larger than pristine Fe_3O_4-based magnetic fluid (6.6 Pa). Furthermore, the particle level dynamic simulation was employed to analyze the microstructure evolution and shear stress of Fe_3O_4@C-based magnetic fluid under applying an external magnetic field. The chain-like model well explained the magnetorheological (MR) mechanism and the simulation results matched perfectly with the experimental data. Since the crystallinity of Fe_3O_4 was improved during the pyrolysis, Fe_3O_4@C nanospheres possessed a higher saturation magnetization. The stronger magnetic dipolar forces and chain-chain interactions resulted in a much steadier Fe_3O_4@C chain-like structure. As a result, it was found that the superior MR performance and high stability of the Fe_3O_4@C-based magnetic fluid were originated from the core-shell and porous structures of Fe_3O_4@C. This work proposed a valuable magnetic particle model to prepare high performance magnetic fluid and further understand the origination of MR effects.

1. Introduction

The magnetic fluids are a category of intelligent materials that compose of magnetic particles and liquid dispersed medium, and their viscosities can be tuned quickly and reversibly by applying the external magnetic field [1]. Because of the magnetic dipole-dipole interactions, the magnetic particles form a chain-like microstructure along magnetic field direction, which lead the magnetic fluids to be transformed from fluid-like to solid-like state. So, the mechanical properties of magnetic fluids change significantly under the external magnetic field [2,3]. Due to the superior rheological behaviour and controllable mechanical properties, magnetic fluids have received a great deal of focuses in diverse application fields, such as intelligent sensors [4], dampers [5,6], exercise industry [7,8] and biological field [9,10], etc.

During the past decades, massive efforts have been made to develop the high-performance magnetic fluids. A variety of magnetic particles, such as ferrite [11–13], carbonyl iron [14,15], chromium dioxide [16] and Fe_3O_4 [17,18] have been used in magnetic fluids. It is generally cognized that MR effect results from the transition of magnetic particles-assembly-structure from disordered to ordered under the external magnetic field. So the morphology, magnetic property, size and inner-structure of magnetic particles exhibit critical influence on the rheological properties [19]. Magnetic particles with various shape such as cubic [20], octahedral [21], rodlike [22] and spherical [23,24] have been developed for magnetic fluids. In comparison to the spherical particles, the anisotropic particles can assemble into stronger chains structure because of their larger friction force [25]. Furthermore, recent studies have manifested that the magnetically induced bundle wire-like structures originated from the magnetic chains were more stable than that of the magnetic nanospheres, therefore the magnetic chains based magnetic fluid possessed preferable MR effect [26]. The inner-structure of magnetic particles plays a one of critical roles for the MR properties. Owing to the low intensity, the hollow magnetic particles endow the final magnetic fluid with high stability. The friction, blocking, and water encapsulation in the hollow structure also strengthen the chain-like structure, thus the hollow magnetic particles show higher MR

* Corresponding authors.
E-mail addresses: jiangwq@ustc.edu.cn (W. Jiang), gongxl@ustc.edu.cn (X. Gong).
[1] The two authors contributed equally to this work

https://doi.org/10.1016/j.jmmm.2020.166734
Received 11 September 2019; Received in revised form 17 January 2020; Accepted 10 March 2020
Available online 10 March 2020
0304-8853/

performance [27,28]. Moreover, the particles size of magnetic particles also affect the mechanical properties of the magnetic fluid. The research indicates that MR effects enhanced with increasing of the particle size and surface interaction [29]. To this end, it is meaningful to investigate the effect of particle nanostructure on the rheological properties.

Recently, the Fe_3O_4-based magnetic fluids have received increasing interests due to its compatible surface, adjustable size and low density which match well with the carrying fluid [30]. The Fe_3O_4 with different size, shape, magnetic property and surface state can be prepared conveniently [29,31–33]. Thus the Fe_3O_4 based magnetic fluid is beneficial to understanding the mechanism of the MR effects by easily tuning the effects of various parameters of magnetic particles [34]. Hence, the investigation of Fe_3O_4 based magnetic fluid is greatly attractive not only for its widely application but also as an ideal candidate for comprehending the MR mechanism. Unfortunately, in previous study, few works have been reported that how the surface state of Fe_3O_4 particles influence the mechanical properties of magnetic fluids. To further understand the mechanism of magnetic fluid and prepare high performance magnetic fluid, it is essential to study the magnetic fluid based on Fe_3O_4 particles with different inner-structure.

In this work, the Fe_3O_4@C nanospheres, which were synthesized *via* pyrolyzing the Fe_3O_4@PDA core-shell nanospheres, could be dispersed into the aqueous solution to prepare high performance magnetic fluid. The rheological testing indicated that the Fe_3O_4@C-based magnetic fluid possessed high MR effect and good stability. In comparison to pristine Fe_3O_4 and Fe_3O_4@PDA particles, the Fe_3O_4@C-based magnetic fluid presented a higher MR performance. Furthermore, the particle level dynamic simulation was applied to analyse the magnetic responds of the magnetic fluid based on Fe_3O_4@C nanospheres. The simulated chain-like model and shear stress as a function of magnetic field agreed well with the experimental data. Finally, a feasible mechanism was proposed to analyse the reasons for the enhancement MR performance of Fe_3O_4@C-based magnetic fluid. This work supplied valuable information for designing high performance magnetic fluid and understanding the MR mechanism.

2. Results and discussion

2.1. Characterization of magnetic Fe_3O_4@C nanospheres

The synthesis procedure sketch of Fe_3O_4@C is exposited in Fig. 1a. Firstly, the Fe_3O_4 nanospheres are prepared *via* a solvothermal reaction [35]. The transmission electronic microscopy (TEM) and scanning electron microscope (SEM) images in Fig. 1b and c indicate that Fe_3O_4 nanoparticles are monodispersed with uniform spherical morphology. The average size of Fe_3O_4 is about 100 nm. From SEM image of Fe_3O_4, it is obviously seen that the surface of Fe_3O_4 is very rough because the Fe_3O_4 nanosphere is composed of numerous small nanocrystals and exhibits a typical cluster-like nanostructure. Then, the PDA shell are equably coated on the surface of Fe_3O_4 through the simple oxidation polymerization, due to its brilliant ability in adhesion to both organic and inorganic substrates. After the decoration of PDA layer, the Fe_3O_4@PDA composite materials still maintain a monodisperse spherical morphology (Fig. 1d and e). From the high magnification TEM image of Fe_3O_4@PDA (inset of Fig. 1d), there is an evident pale layer located at the periphery of Fe_3O_4. Additionally, the surface of Fe_3O_4@PDA (Fig. 1e) is smoother than that of Fe_3O_4 and the average size of Fe_3O_4@PDA nanospheres increases to about 110 nm. All of results prove the existence of uniform PDA layer. After PDA shell being carbonized to carbon shell, the Fe_3O_4@PDA transform to Fe_3O_4@C nanospheres. The Fe_3O_4@C nanospheres show spherical morphology without apparent aggregation, which gives the credit to the presence of PDA shell (Fig. 1f and g). Interestingly, the average size of Fe_3O_4@C is about 100 nm, which is a little smaller than the Fe_3O_4@PDA precursor. Form the high magnification TEM image (inset of Fig. 1f), it can be observed that the Fe_3O_4@C nanospheres possess porous structures. The Brunauer-Emmett-Teller (BET) surface area of Fe_3O_4@C is 66.8 m^2/g, which is higher than that of Fe_3O_4 (50.8 m^2/g) (Fig. S2). After carefully comparing the TEM images of Fe_3O_4 and Fe_3O_4@C (Fig. 1b and f), it can be observed that the Fe_3O_4 nanograins sizes get bigger after the pyrolysis process.

X-ray photoelectron spectroscopy (XPS) is performed to examine the shell structure of the final products. As exhibited in Fig. 2a, the signals of Fe, O and C elements are clearly detected in the XPS spectrum of Fe_3O_4, which are originated from the Fe_3O_4 and residual polymer reagents. After being covered by PDA shell, the specific signal of N 1s is found and the intensity of C 1s is enhanced in the corresponding curve, demonstrating that PDA layer is wrapped on the Fe_3O_4 core successfully. Furthermore, Fe 2p and Fe 3p signals still exist but the signal intensities of them are reduced significantly, thus the thickness of PDA layer is less than 10 nm because the detection thickness of the XPS is about 10 nm, which is in accordance with the TEM analysis. The C1s core-level spectrum of Fe_3O_4@PDA shows four characteristic peaks at 288.75, 287.9, 286.15 and 284.8 eV, which can be assigned to O–C = O, C = O, C–N, C = C, respectively (Fig. 2b). The N 1s spectrum can be split to three peaks at 401.95, 400.1 and 398.45 eV (Fig. 2c). The first peak at 401.95 eV corresponds to the amine group (R-NH_2), which must come from the small amount of physically self-assembled dopamine. The peaks at 400.1 and 398.45 eV can be ascribed to the substituted amine (–N–H) and imino (= N–R) groups of PDA. The wide-scan XPS spectrum of Fe_3O_4@C is similar to that of Fe_3O_4@PDA, because the Fe_3O_4@C is obtained by the pyrolysis of Fe_3O_4@PDA. Nevertheless, the C 1s and N 1s core-level spectra of Fe_3O_4@C (Fig. 2b and c) is slightly different from that of Fe_3O_4@PDA. After pyrolysis, the intensity of C = C and imino (= N–R) peaks are apparently increased, which can be attributed to the formation of graphite carbon.

The Raman spectra further prove the presence of PDA and C layer. As shown in Fig. 3a, there are two visible peaks at 1582 and 1368 cm^{-1}, corresponding to the G and D bands, respectively. After the pyrolysis, the crystallization of the carbon component in the Fe_3O_4@C is better than the Fe_3O_4@PDA, thus sharper peaks are found in the Raman spectra. Moreover, it can be distinctly observed that the weight loss of Fe_3O_4@C (9.9%) is much lower than that of Fe_3O_4@PDA (20.6%) and higher than that of Fe_3O_4 (6.8%) (Fig. 3b). All results indicate that there is a thin carbon layer on the surface of Fe_3O_4 in the Fe_3O_4@C.

The XRD patterns are applied to track the synthetic process of the Fe_3O_4@C nanospheres. As shown in Fig. 3c, all the products show the pure face-cubic centred magnetite phase of the Fe_3O_4, because the crystal phase in Fe_3O_4, Fe_3O_4@PDA and Fe_3O_4@C is Fe_3O_4. Based on the Scherrer formula, the nanograins sizes of Fe_3O_4 and Fe_3O_4@C are calculated to be 10 and 15 nm, respectively. This result indicates the crystallinity of Fe_3O_4 is critically improved during the pyrolysis process, which is keeping with the TEM images analyses.

The magnetic properties of as-prepared samples are evaluated by SQUID at room temperature. The hysteresis loop of each sample presents the typical superparamagnetic characteristic, of which the coercivity (Hc) and remanent magnetization are almost zero (Fig. 3d). Therefore, these nanopheres are easy to be dispersed to form homogenous solution. All samples can be completely saturated at an external magnetic field of 20 KOe. The saturation magnetizations of Fe_3O_4, Fe_3O_4@PDA and Fe_3O_4@C are 69.8, 52.6 and 69.8 emu/g, respectively. There is no doubt that the magnetic properties of each sample are derived from the Fe_3O_4 core, because the PDA and C shell are non-magnetic. The introduction of non-magnetic material reduces the saturation magnetization of the target product but the saturation magnetization of Fe_3O_4@C is as high as original Fe_3O_4, indicating that the saturation magnetization of Fe_3O_4 component in Fe_3O_4@C is higher than original Fe_3O_4. Combining the TG analysis, the saturation magnetization of Fe_3O_4 in Fe_3O_4@C is 80.4 emu/g.

In this work, to explore the influence of shell modification, the resorcinol/formaldehyde resin (RF) and SiO_2 modified magnetic particles

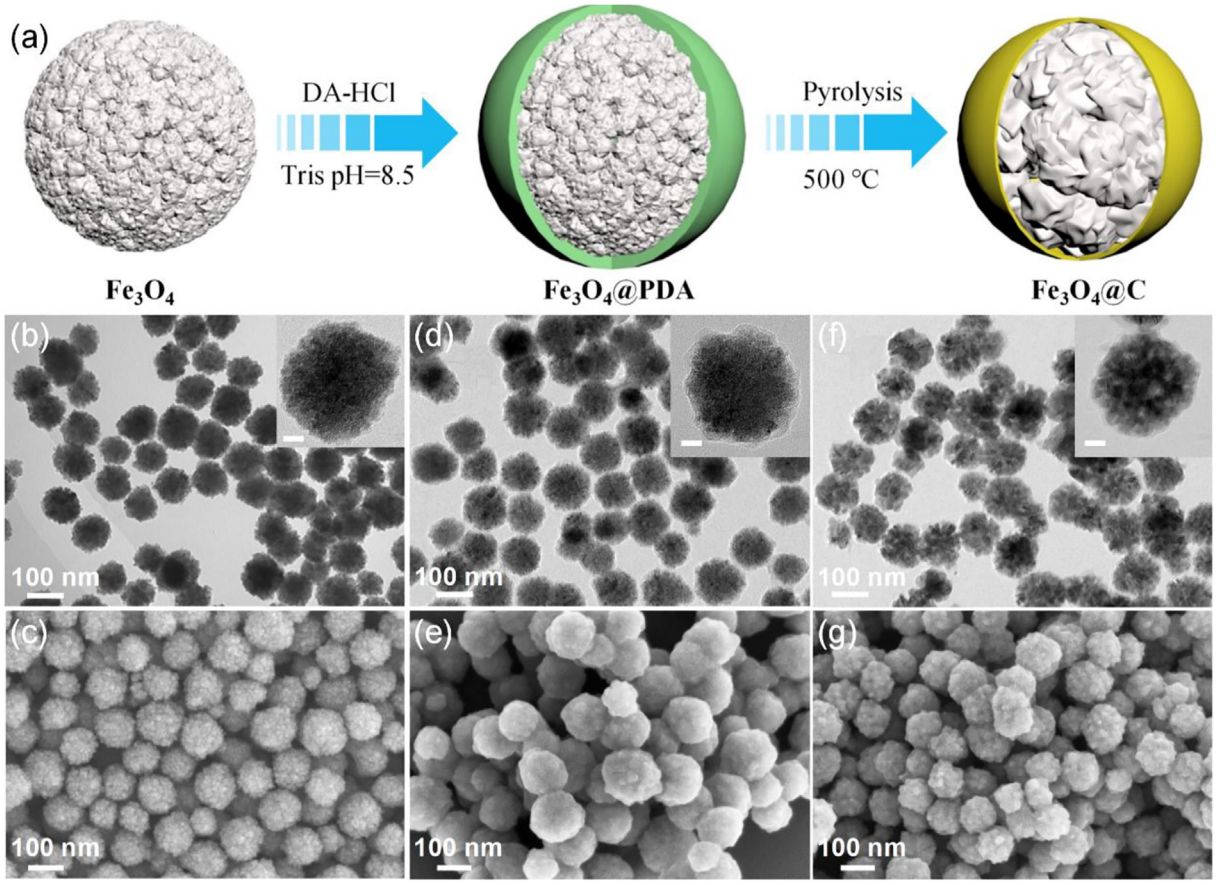

Fig. 1. Synthesis procedure sketch of the Fe_3O_4@C (a), transmission electronic microscopy (TEM) and scanning electron microscope (SEM) images of Fe_3O_4 (b, c), Fe_3O_4@PDA (d, e), Fe_3O_4@C (f, g). (inset) Corresponding TEM images with high magnification (the plotting scale is 60 nm).

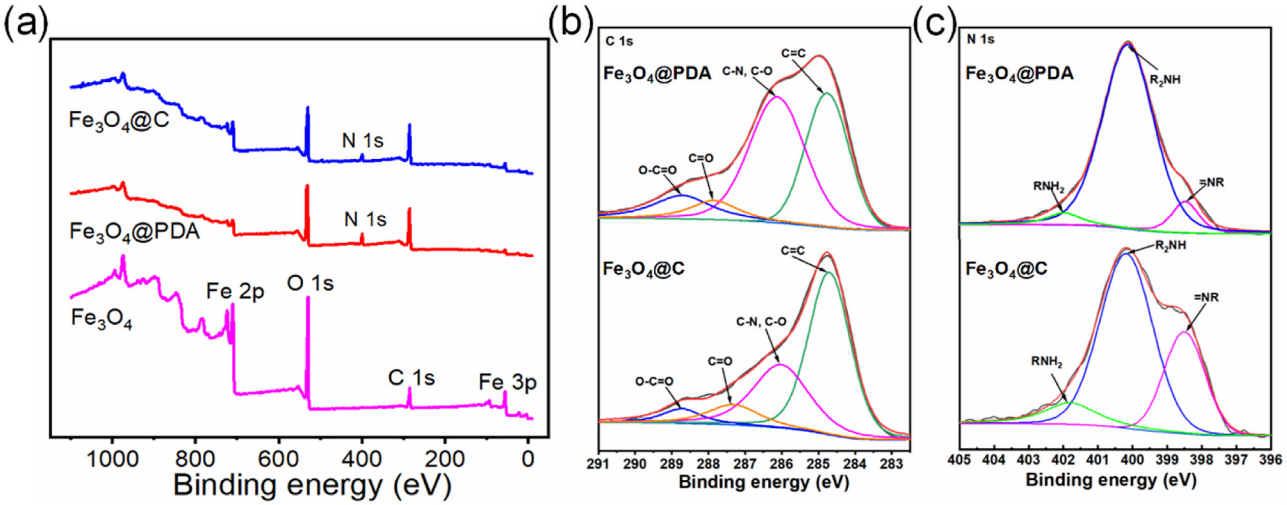

Fig. 2. X-ray photoelectron spectroscopy (XPS) of Fe_3O_4, Fe_3O_4@PDA and Fe_3O_4@C (a), C 1s core-level spectra of Fe_3O_4@PDA and Fe_3O_4@C (b), N 1s core-level spectra of Fe_3O_4@PDA and Fe_3O_4@C (c).

as contrast samples are also synthesized. A series of characterizations of Fe_3O_4@RF and Fe_3O_4@SiO_2 particles are carried out, including TEM, SEM, XPS, TG and magnetization hysteresis loops (Figs. S3–S5). Meanwhile, the mechanical properties of Fe_3O_4@RF and Fe_3O_4@SiO_2-based magnetic fluids are investigated and the relevant descriptions are in the supplementary material (Fig. S6).

2.2. Magneto-responsive rheological characteristics of magnetic fluids based on different magnetic core-shell nanospheres

Magnetic fluids are prepared by dispersing Fe_3O_4, Fe_3O_4@PDA and Fe_3O_4@C nanospheres into deionized water, respectively. Here, the weight ratio of the magnetic particles is all kept at 10 wt%. The rheological activities of magnetic fluids are investigated by commercially available rheometer (Physia MCR302, Anton Paar) and the magnetic field is applied *via* the magnetorheological unit. Fig. 4a–c show the

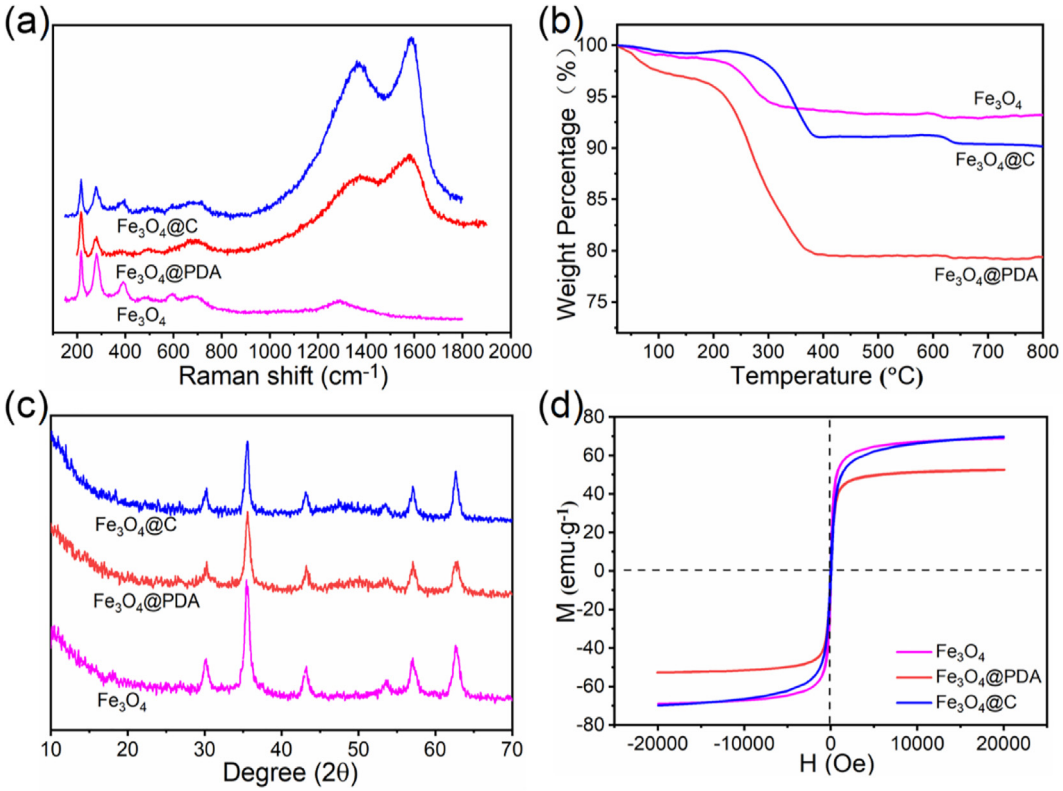

Fig. 3. Raman spectra (a), Thermogravimetry (TG) curves (b), X-Ray Diffraction (XRD) patterns (c) and Magnetization hysteresis loops (d) of Fe_3O_4, Fe_3O_4@PDA and Fe_3O_4@C.

typical shear stress *vs* shear rate curves of as-prepared magnetic fluids. When the applied magnetic field is 0 mT, the shear stress of as-prepared magnetic fluid increases upon increasing the shear rate, which is consistent with the Newtonian fluid (Fig. 4a–c). Under applying constant magnetic field, the shear stress increases with increasing of the shear rate which is similar to traditional magnetic fluids (Fig. 4a–c). Additionally, under applying the external magnetic field, the shear stress of magnetic fluids is substantially enhanced, which is ascribed to the formation of chain-like structure aligned in the magnetic direction. As shown in Fig. 4a and b, the shear stress of Fe_3O_4 and Fe_3O_4@PDA-based magnetic fluid increases with increasing of magnetic flux density from 0 to 110 mT. When the magnetic flux density reaches to 220 mT, the shear stress of these two magnetic fluids are reduced. But the shear stress of Fe_3O_4@PDA-based magnetic fluid declines slowly. For Fe_3O_4@C-based magnetic fluid, the shear stress values decrease until the magnetic field attains to 440 mT (Fig. 4c). The decline of shear stress values is possibly due to the agglomeration of nanospheres, indicating that the Fe_3O_4@C-based magnetic fluid is more stable.

Furthermore, the larger magnetic field usually results in a higher shear stress. Fig. 4d shows the magnetic field dependent shear stress of magnetic fluids composed of Fe_3O_4, Fe_3O_4@PDA and Fe_3O_4@C nanospheres, respectively. Clearly, the shear stress rapidly increases with the enhancement of magnetic field at initial phase, proving the characteristic MR effects. It is apparent that the Fe_3O_4@C-based magnetic fluid possesses higher shear stress than other magnetic nanospheres. The Fe_3O_4@C-based magnetic fluid is nearly saturated at 180 mT while Fe_3O_4 and Fe_3O_4@PDA based magnetic fluids are almost saturated at 60 mT. The magnetic induced shear stress values for Fe_3O_4, Fe_3O_4@PDA and Fe_3O_4@C-based magnetic fluid are calculated to be 6.6, 6.4 and 24.9 Pa, respectively (Fig. 4d). In addition, the shear stress decreases with further increasing the magnetic field, which is in accordance with the information exhibited in Fig. 4a–c. The interaction force between magnetic dipoles increase with the increasing of the magnetic field. While the magnetization intensity of particles is saturated, the interaction force will no more increment with the magnetic field increased. Therefore, the shear stress increases quickly when the magnetic field is lower than saturation magnetization. Besides, the mass fraction of all samples is kept at 10 wt% which is quite low, and the particles might tend to assemble in the center of the plate with the application of external magnetic field. Furthermore, because of the low viscosity of water, it is inevitable to exist sealing effect which lead to a reduction in the number of the magnetic field-induced particles chain at high magnetic field, hence the shear stress is decreased.

In previous works, various particles were used for preparing magnetic fluids. In comparison to Fe_3O_4 nanospheres, the Fe_3O_4@C-based magnetic fluid shows preferable MR effect. It is well known that MR effect increases with increasing the particle size. The magnetic induced shear stress value of Fe_3O_4@C-based magnetic fluid (24.9 Pa) is even higher than that of MRF-200 (12 Pa), in which the magnetic fluid consists of 200 nm Fe_3O_4 nanospheres [29]. In comparison to hollow magnetite ferrofluids, the Fe_3O_4@C-based magnetic fluid also possesses superior MR property, which is higher than the Fe_3O_4 hollow spheres and chain-based magnetic fluid [26]. However, when the diameter of hollow spheres rises to 300 nm, the MR effect of hollow nanospheres is stronger [28]. To sum up, the decoration of carbon layer endows magnetic particles with stronger MR performance. Here, the Fe_3O_4@C particles also equip with abundant porous structure and high surface area, which help the magnetic fluid possesses high stability. Furthermore, the carbon shell can serve as protective layer, which is beneficial to restrain the oxidization of magnetic particles.

Particle level dynamic simulations are carried out to investigate the correlation between microstructures and MR effect of magnetic fluid. Typical rearrangement of Fe_3O_4@C particles in steady shear flow is firstly discussed using the OVITO software [36] (Fig. 5a). In this section, a steady uniform magnetic field of B = 200 mT is chosen as an example. Such magnetic field can ensure the magnetic fluid exhibit the maximum MR effect. The shear rate and weight fraction of magnetic fluid are set at 10 s^{-1} and 10 wt%, corresponding to the rheological

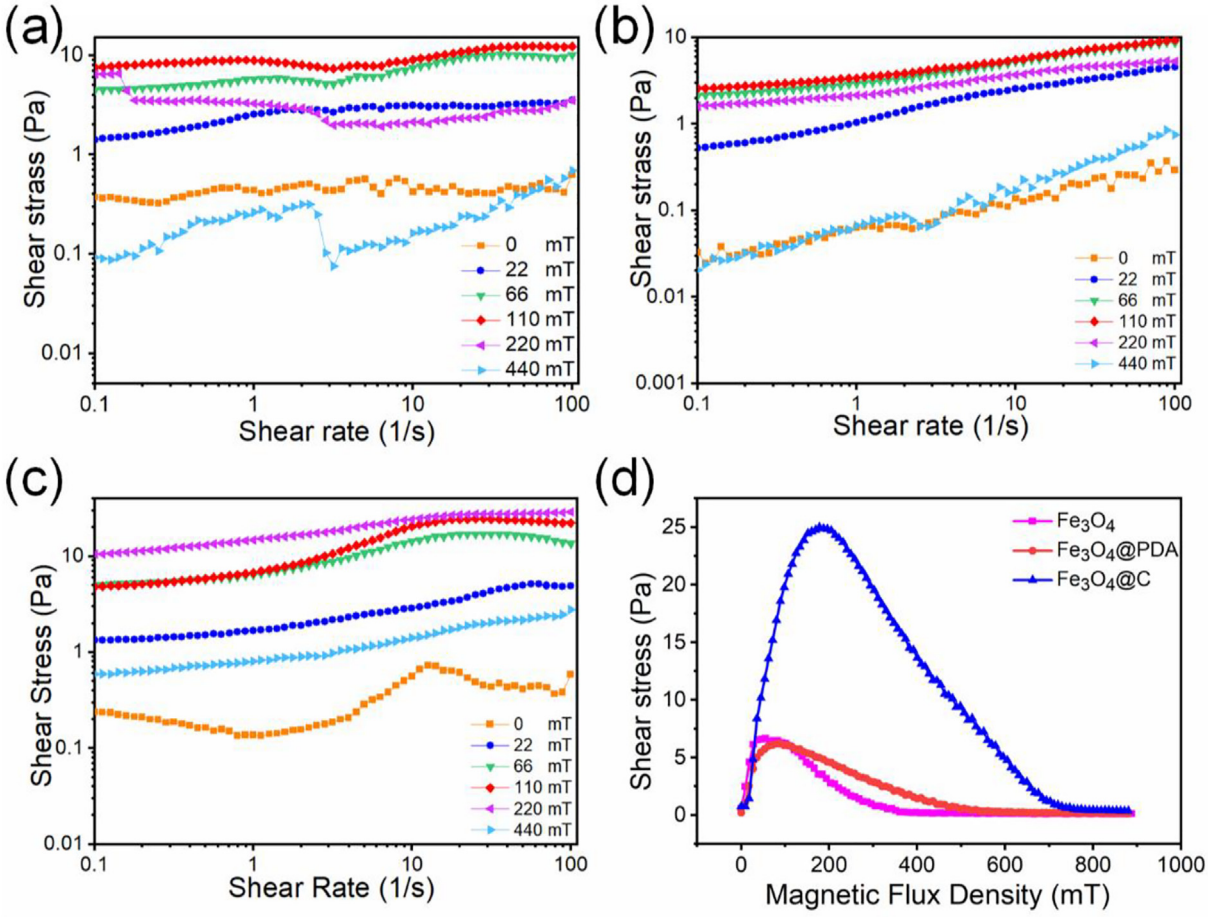

Fig. 4. Shear stress *vs* shear rate curves of magnetic fluids based on Fe_3O_4 (a), Fe_3O_4@PDA (b) and Fe_3O_4@C (c) nanospheres, respectively. Magnetic field dependent shear stress of magnetic fluids composed of corresponding Fe_3O_4-based nanospheres (d).

tests. At the initial state, Fe_3O_4@C particles are randomly distributed in the simulation box. After applying the external magnetic field and shear flow for 0.2 ms, particles rapidly form short chains along the field direction due to the magnetic dipolar forces. At 0.4 ms, short chains arrange head-to-tail to form longer chain-like microstructures. With the development of shear flow, chain-like microstructures then incline toward different directions at 10 ms. Dip angles of chains are quite small. In such configuration, the x-component of magnetic dipolar forces are balanced with the hydrodynamic force from the matrix. When the magnetic fluid reaches dynamic equilibrium (40 ms), chain-like microstructures slightly move around the original position due to the Brownian force. Those chains don't flow with the matrix or further aggregate into other particular microstructures during the simulation. Microstructures in dynamic equilibrium under different external fields are plotted in Fig. 5b. Chain-like microstructures possess a consistent slope toward the shear direction (x-axis) under a weak magnetic field

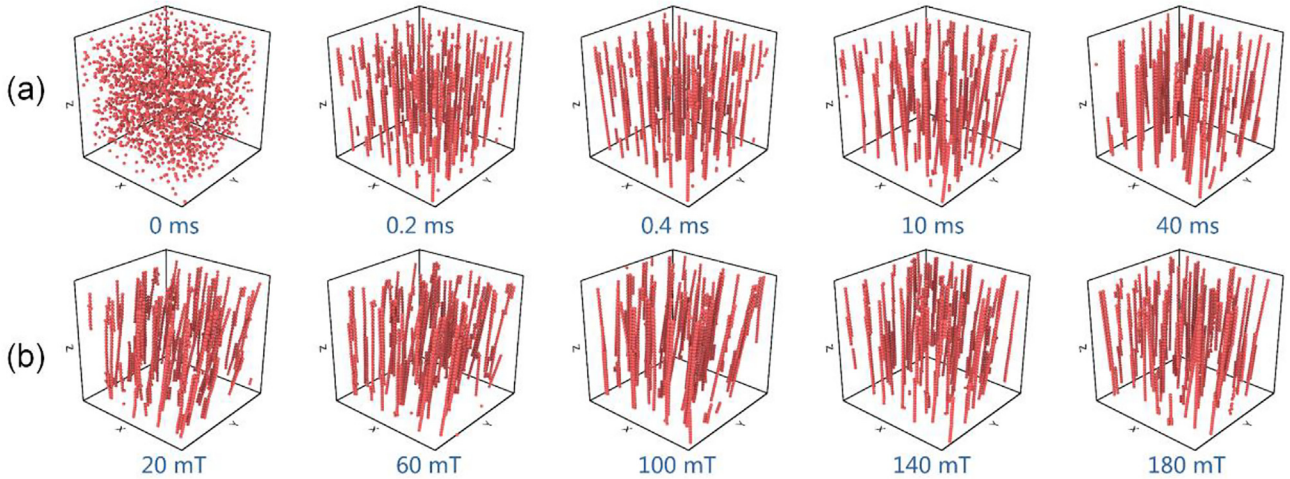

Fig. 5. Evolution of microstructures of Fe_3O_4@C particles under a magnetic field of 200 mT (a), Microstructures of Fe_3O_4@C particles at the end of the simulations under different magnetic fields (b).

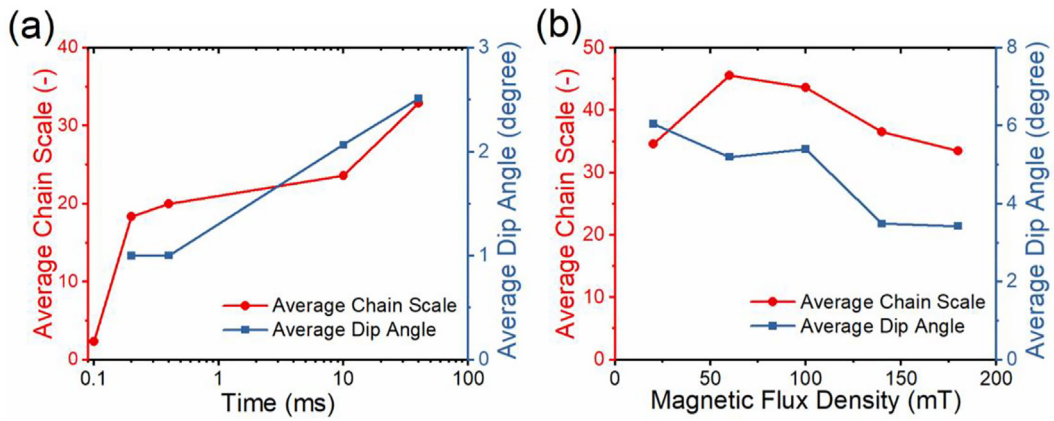

Fig. 6. Average chain Scale and average dip angle of microstructures of Fe_3O_4@C magnetic fluid at 0.1, 0.2, 0.4, 10, and 40 ms under a 200 mT magnetic field (a); at 40 ms under a magnetic of 20, 60, 100, 140, and 180 mT (b). The lines are plotted to guide the eyes. The weight fraction of the particle is 10 wt%.

(20 mT). The dip angle of chains decreases and become irregular with increasing the external field. If the magnetic field strength exceeds 140 mT, microstructures show familiar characteristics. The x-component of magnetic dipolar forces is in positive correlation with both the magnetic flux density and the inclination of microstructures. Under the same shear rate, the stronger external magnetic field, the small dip angle of chains is required to resist the shear flow.

In the simulations, if the distance between two particles was smaller than 1.2d (d = 100 nm), these two particles are considered in the same chain. The dip angle of the chain is defined as the angle between the axis of chain and the external field. The average scale of chains increases from 2.3 to 32.9 particles with the development of shear flow, while the average dip angle increases from 0.99 to 2.51 degrees under a 200 mT magnetic field (Fig. 6a). At the initial state, most of the particles are isolated. The dip angle of chains is meaningless at this time. After applying the magnetic field and shear flow, isolate particles and large chain-like microstructures always exist at the same time. The microstructures are usually not single-particle-width chains. The disparity between the biggest and smallest chains is quite large. The largest chain contains 79 particles and the dip angle varies from 0.23 to 12.53 degrees at the end of the simulation. The average scale of chains at the end of the simulation increases and then declines when increasing the external field (Fig. 6b). The maximum average scale was 46 particles. The average scale under 20 and 180 mT were approximately the same (Fig. 6b). The dip angle of chains exhibits a decreasing trend from 6.0 to 3.4 degrees with increasing the magnetic field, which is consistent with the snapshot of microstructures (Fig. 5).

Meanwhile, the simulated shear stress as a function of magnetic flux density is also discussed (Fig. 7). Shear stress first linearly increases with the external field and reaches saturation after B = 150 mT. A good correspondence between simulations and experiments is observed, which confirms the particle-level simulation method has a high accuracy. Simulated shear stress of magnetic fluid based on Fe_3O_4@C particles is also stronger than the experimental shear stress of pure Fe_3O_4 magnetic fluid. The microstructure evolution of Fe_3O_4@C-based magnetic fluid is similar the one prepared by Fe_3O_4 particles. The improvement of magnetic moment of Fe_3O_4@C particles induces larger shear stress than the Fe_3O_4 particles.

The changing processes of magnetic fluids based on Fe_3O_4 and Fe_3O_4@C nanospheres from a random status to chain-like structure are displayed in Fig. S7. When an external magnetic field is applied, the random dispersed particles in magnetic fluid assemble to form chain-like structure along the direction of magnetic field. With the exerting of steady shear, the chains tilt with quite small dip angles. This process is depended on the acting force between the magnetic particles. Fig. 8a presents the force analyses of magnetic fluids based on Fe_3O_4 and Fe_3O_4@C nanospheres, respectively. The Fe_3O_4@C possesses higher

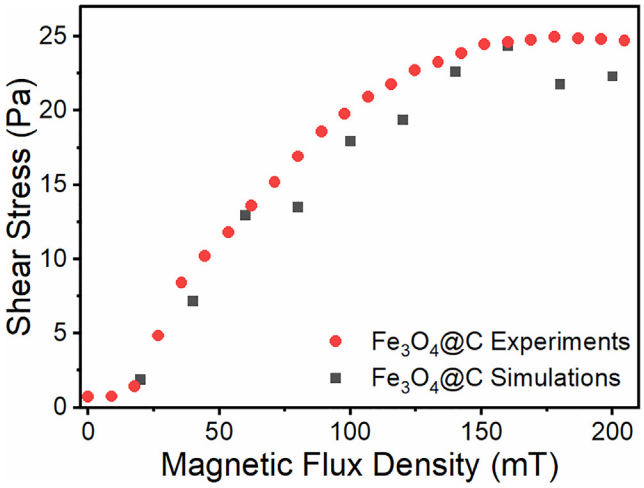

Fig. 7. Shear stress as a function of magnetic flux density, a comparison between experiments and simulations.

crystallinity and shows bigger magnetic torque, which leads to stronger magnetic dipolar forces. The enhanced magnetic dipolar forces and unique properties of Fe_3O_4@C greatly strengthen the as-formed chain-like structures, thus the Fe_3O_4@C-based magnetic fluid has a larger MR effect than that of Fe_3O_4.

To further verify the inference, the actual chain-like structure of magnetic fluid are observed in a Poiseuille flow. As shown in Fig. 8c, the microfluidic channel is manufactured in a slice of polydimethylsiloxane (PDMS) with a 280 μm × 120 μm rectangular section. A permanent magnet is parallelly placed to the channel to generate a homogeneous magnetic field. The volume flow is set to 0.5 ml/h and the frame rate of high-speed camera is 20,000 fps. From Fig. 8b it can be seen that Fe_3O_4 and Fe_3O_4@C-based magnetic fluid both form chains-like structure parallel to the magnetic field, which are consistent with the simulation results. In contrast to the Fe_3O_4, the Fe_3O_4@C fluid (Fig. 8b (II)) shows thicker and sparse particle chains structure, which is attributed to stronger interaction forces between Fe_3O_4@C particles. So the Fe_3O_4@C based magnetic fluid exhibits much better MR properties.

3. Conclusion

In this work, a novel kind of Fe_3O_4@C magnetic particles are prepared by surface modification. These Fe_3O_4@C particles are dispersed into water to prepare magnetic fluid and its rheological properties are measured. Fe_3O_4@C-based magnetic fluid shows better mechanical properties than the pristine Fe_3O_4 and Fe_3O_4@PDA particles. It is found

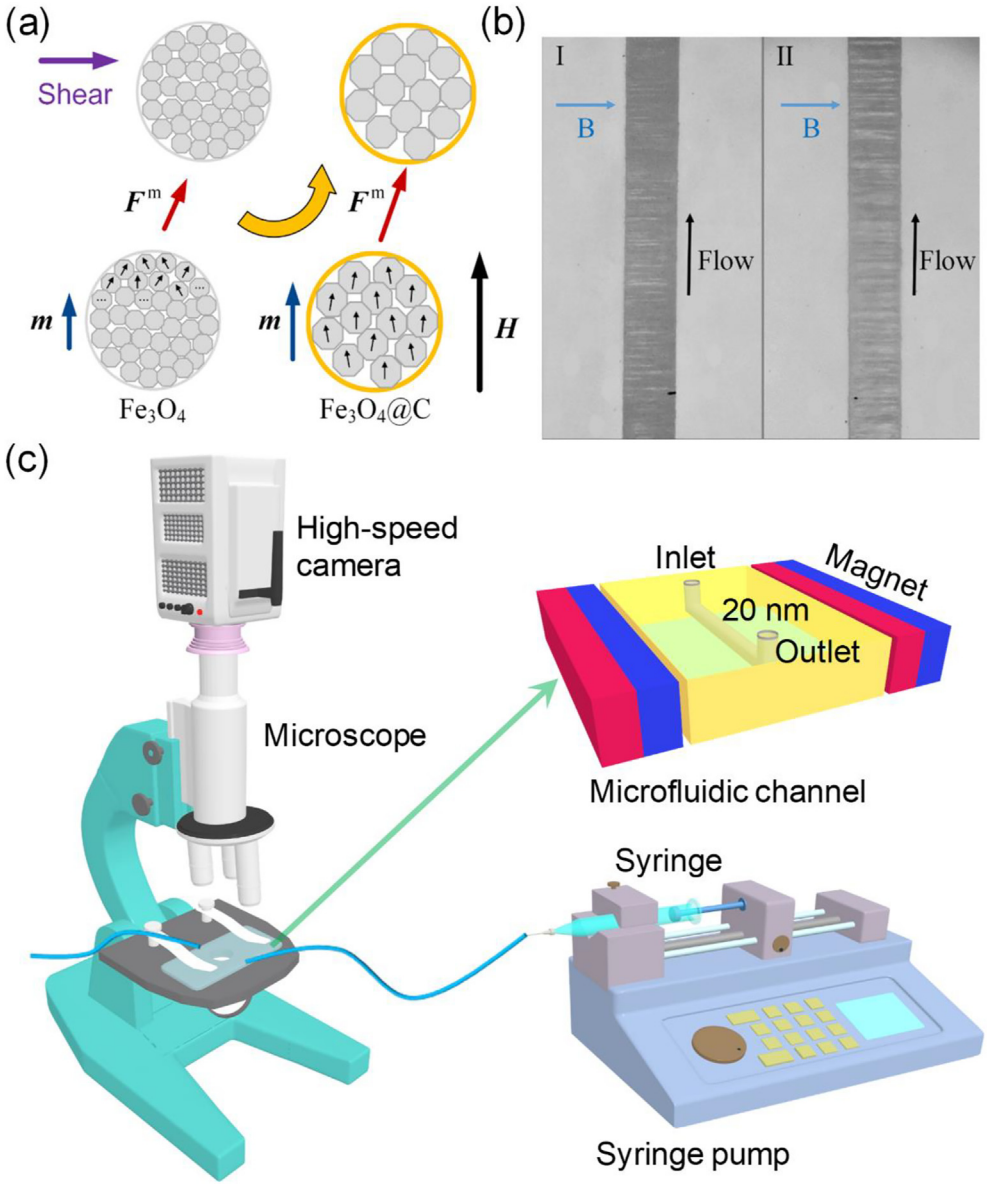

Fig. 8. Force analyses of magnetic fluid based on Fe_3O_4 and Fe_3O_4@C nanospheres (a), Snapshots of magnetic fluid based on Fe_3O_4 (I) and Fe_3O_4@C (II) in Poiseuille flow in a microfluidic channel (b), schematic diagram of the microfluidic channel and experimental setup (c).

that the carbon layer and unique porous inner-structure of Fe_3O_4@C play critical roles in determining the MR effects of the final magnetic fluid. Furthermore, the Particle level dynamic simulations about microstructure evolution and magnetic field dependent shear stress are carried out. The chain-like model well explains the MR mechanism and the simulation results matches perfectly with the experimental data. Due to the stronger magnetic dipolar forces, chain-chain interaction and much steadier chain-like structure, the Fe_3O_4@C-based magnetic fluid exhibits enhanced MR effects. This work is valuable for researcher to further prepare high performance magnetic fluid and understand the origination of MR effects.

CRediT authorship contribution statement

Linfeng Bai: Investigation, Formal analysis, Resources, Writing - original draft. **Lei Pei:** Software. **Saisai Cao:** Investigation. **Xiaokang He:** Investigation. **Min Sang:** Writing - review & editing. **Wanquan Jiang:** . **Shouhu Xuan:** Conceptualization, Writing - review & editing, Supervision. **Xinglong Gong:** .

Declaration of Competing Interest

The authors declare that they have no known competing financial interests or personal relationships that could have appeared to influence the work reported in this paper.

Acknowledgements

Financial supports from the National Natural Science Foundation of China (Grant No. 11822209, 11572310), and the Strategic Priority Research Program of the Chinese Academy of Sciences Grant No. XDB22040502 are gratefully acknowledged. This study was also supported by the Collaborative Innovation Center of Suzhou Nano Science and Technology.

Appendix A. Supplementary data

Supplementary data to this article can be found online at https://doi.org/10.1016/j.jmmm.2020.166734.

References

[1] J. de Vicente, D.J. Klingenberg, R. Hidalgo-Alvarez, Magnetorheological fluids: a review, Soft Matter 7 (2011) 3701–3710.

[2] I. Bica, E.M. Anitas, Q. Lu, H.J. Choi, Effect of magnetic field intensity and γ-Fe_2O_3 nanoparticle additive on electrical conductivity and viscosity of magnetorheological carbonyl iron suspension-based membranes, Smart Mater. Struct. 27 (2018) 095021.

[3] Y.P. Seo, S. Han, J. Choi, A. Takahara, H.J. Choi, Y. Seo, Searching for a stable high-performance magnetorheological suspension, Adv. Mater. 30 (2018) 1704769.

[4] G. Huang, B. Zhou, Z. Chen, H. Jiang, X. Xing, Magnetic-field sensor utilizing the ferrofluid and thin-core fiber modal interferometer, IEEE Sens. J. 15 (2015) 333–336.

[5] D.-S. Yoon, Y.-J. Park, S.-B. Choi, An eddy current effect on the response time of a magnetorheological damper: analysis and experimental validation, Mech. Syst. Signal Pr. 127 (2019) 136–158.

[6] J. Yang, S. Sun, W. Li, H. Du, G. Alici, M. Nakano, Development of a linear damper working with magnetorheological shear thickening fluids, J. Intel. Mat. Syst. Str. 26 (2015) 1811–1817.

[7] V. Grigas, A. Sulginas, P. Ziliukas, Development of magnetorheological resistive exercise device for rowing machine, Comput. Math. Methods Med. (2016) 1–14.

[8] S. Dong, K.Q. Lu, J.Q. Sun, K. Rudolph, Adaptive force regulation of muscle strengthening rehabilitation device with magnetorheological fluids, IEEE Trans. Neural. Syst. Rehabil. Eng. 14 (2006) 55–63.

[9] B.J. Park, F.F. Fang, H.J. Choi, Magnetorheology: materials and application, Soft Matter 6 (2010) 5246–5253.

[10] F. Pineux, R. Marega, A. Stopin, A. La Torre, Y. Garcia, E. Devlin, C. Michiels, Biotechnological promises of Fe-filled CNTs for cell shepherding and magnetic fluid hyperthermia applications, Nanoscale 7 (2015) 20474–20488.

[11] J.K. Han, H.J. Choi, Non-stoichiometric zinc-doped spinel ferrite nanoparticles with enhanced magnetic property and their magnetorheology, Colloid. Polym. Sci. 296 (2017) 405–409.

[12] A.V. Anupama, V. Kumaran, B. Sahoo, Application of Ni-Zn ferrite powders with polydisperse spherical particles in magnetorheological fluids, Powder Technol. 338 (2018) 190–196.

[13] G. Wang, F. Zhou, Z. Lu, Y. Ma, X. Li, Y. Tong, X. Dong, Controlled synthesis of $CoFe_2O_4/MoS_2$ nanocomposites with excellent sedimentation stability for magnetorheological fluid, J. Ind. Eng. Chem. 70 (2019) 439–446.

[14] P. Zhang, Y.Z. Dong, H.J. Choi, C.-H. Lee, Tribological and rheological tests of core-shell typed carbonyl iron/polystyrene particle-based magnetorheological fluid, J. Ind. Eng. Chem. 68 (2018) 342–349.

[15] I.H. Park, H.J. Choi, Fabrication of p-aminobenzoic acid grafted carbonyl iron/polyindole composite particles and their magnetorheological response, J. Ind. Eng. Chem. 64 (2018) 102–106.

[16] M.H. Kim, K. Choi, J.D. Nam, H.J. Choi, Enhanced magnetorheological response of magnetic chromium dioxide nanoparticle added carbonyl iron suspension, Smart Mater. Struct. 26 (2017) 095006.

[17] Y.Z. Dong, H.J. Choi, Synthesis of smart poly(diphenylamine)/magnetic particle composites and their electric/magnetic stimuli-response, Macromol. Res. 26 (2018) 667–670.

[18] H.S. Chae, S.H. Piao, W.J. Han, H.J. Choi, Core/shell polystyrene/magnetite hybrid nanoparticles fabricated by pickering emulsion polymerization and their magnetorheological response, Macromol. Chem. Phys. 219 (2018) 1700408.

[19] H. Chiriac, G. Stoian, Influence of the particles size and size distribution on the magnetorheological fluids properties, IEEE T. Magn. 45 (2009) 4049–4051.

[20] I. Arief, P.K. Mukhopadhyay, Preparation of spherical and cubic Fe 55 Co 45 microstructures for studying the role of particle morphology in magnetorheological suspensions, J. Magn. Magn. Mater. 360 (2014) 104–108.

[21] S.H. Kwon, H.S. Jung, H.J. Choi, Z. Strecker, J. Roupec, Effect of octahedral typed iron oxide particles on magnetorheological behavior of carbonyl iron dispersion, Colloid. Surfaces A 555 (2018) 685–690.

[22] A.V. Anupama, V. Kumaran, B. Sahoo, Magnetorheological fluids containing rod-shaped lithium-zinc ferrite particles: the steady-state shear response, Soft Matter 14 (2018) 5407–5419.

[23] S.-P. Rwei, J.-W. Shiu, R. Sasikumar, H.-C. Hsueh, Characterization and preparation of carbonyl iron-based high magnetic fluids stabilized by the addition of fumed silica, J. Solid State Chem. 274 (2019) 308–314.

[24] S. Lee, K.Y. Shin, J. Jang, Enhanced magnetorheological performance of highly uniform magnetic carbon nanoparticles, Nanoscale 7 (2015) 9646–9654.

[25] G. Salazar-Alvarez, J. Qin, V. Sepelak, Cubic versus spherical magnetic nanoparticles: the role of surface anisotropy, J. Am. Chem. Soc. 130 (2008) 13234–13239.

[26] S. Xuan, L. Hao, K.C.-F. Leung, Shear disassembly of hierarchical superparamagnetic Fe_3O_4 hollow nanoparticle necklace chains, New J. Chem. 38 (2014) 6125–6132.

[27] J.S. An, W.J. Han, H.J. Choi, Synthesis of hollow magnetite nanoparticles via self-assembly and their magnetorheological properties, Colloid. Surfaces A 535 (2017) 16–23.

[28] X. Ruan, L. Pei, S. Xuan, Q. Yan, X. Gong, The rheological responds of the superparamagnetic fluid based on Fe_3O_4 hollow nanospheres, J. Magn. Magn. Mater. 429 (2017) 1–10.

[29] J. Wu, L. Pei, S. Xuan, Q. Yan, X. Gong, Particle size dependent rheological property in magnetic fluid, J. Magn. Magn. Mater. 408 (2016) 18–25.

[30] H.S. Chae, S.H. Piao, H.J. Choi, Fabrication of spherical Fe_3O_4 particles with a solvothermal method and their magnetorheological characteristics, J. Ind. Eng. Chem. 29 (2015) 129–133.

[31] P. Saha, S. Mukherjee, K. Mandal, Rheological response of magnetic fluid containing Fe_3O_4 nano structures, J. Magn. Magn. Mater. 484 (2019) 324–328.

[32] A.V. Anupama, V.B. Khopkar, V. Kumaran, B. Sahoo, Magnetic field dependent steady-state shear response of Fe_3O_4 micro-octahedron based magnetorheological fluids, Chem. Chem. Phys. 20 (2018) 20247–20256.

[33] D.H. Bae, W.J. Han, C.Y. Gao, Y.Z. Dong, H.J. Choi, Preparation and magnetorheological response of triangular-shaped single-crystalline magnetite particle-based magnetic fluid, IEEE T. Magn. 54 (2018) 1–4.

[34] L. Pei, H. Pang, K. Chen, S. Xuan, X. Gong, Simulation of the optimal diameter and wall thickness of hollow Fe_3O_4 microspheres in magnetorheological fluids, Soft Matter 14 (2018) 5080–5091.

[35] Q. Fang, J. Zhang, L. Bai, J. Duan, H. Xu, K. Cham-Fai Leung, S. Xuan, In situ redox-oxidation polymerization for magnetic core-shell nanostructure with polydopamine-encapsulated-Au hybrid shell, J. Hazard. Mater. 367 (2019) 15–25.

[36] A. Stukowski, Visualization and analysis of atomistic simulation data with OVITO-the open visualization tool, Modell. Simul. Mater. Sc. 18 (2009) 015012.